Supplementary information

Interstitial anionic electrons as spin–charge reservoirs for sterically tuned single-atom catalysis in 2D electrides

Huimin Hu,[a,b] and Jin-Ho Choi,[a,b] *

[a]*College of Energy, Soochow Institute for Energy and Materials InnovationS, Soochow University, Suzhou 215006, China*

[b]*Key Laboratory of Advanced Carbon Materials and Wearable Energy Technologies of Jiangsu Province, Soochow University, Suzhou 215006, China*

*e-mail: jhchoi@suda.edu.cn

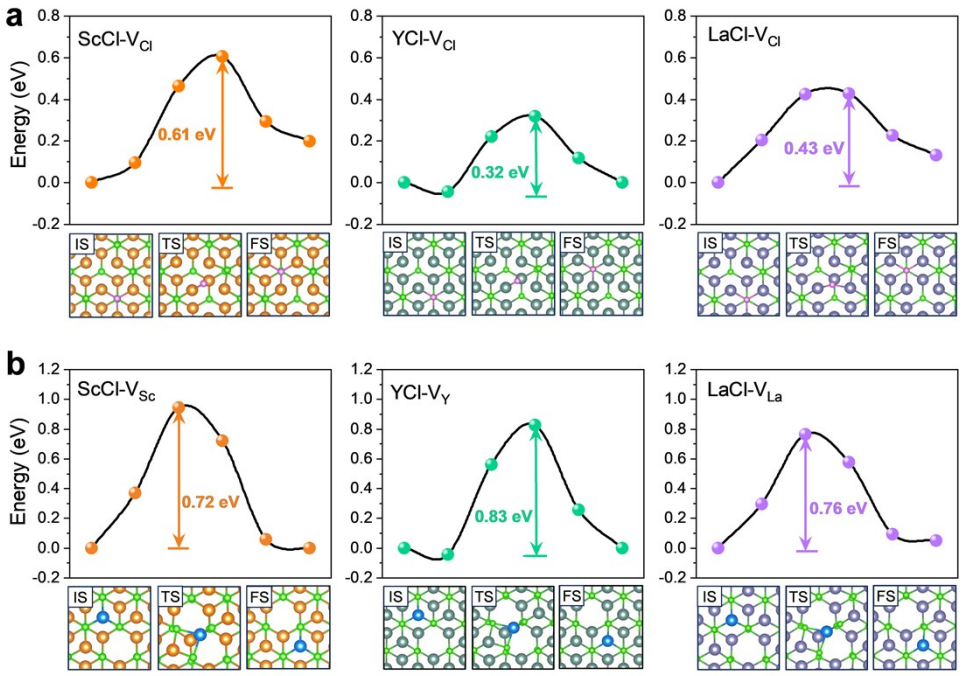

Fig. S1 NEB energy profiles for vacancy migration**.** (a) V_{Cl} and (b) V_X in ScCl (left), YCl (middle) and LaCl (right). The initial (IS), transition (TS) and final-state (FS) configurations during process are displayed at bottom. The migrated V_{Cl} and V_X are highted by pink and blue circles.

The removal of an X^{3+} cation eliminates a strong positive electrostatic center, significantly raising the local potential at the neighboring IAEs-A site (A1). This destabilizes electron confinement, causing majority-spin electrons to partially delocalize from A1. Meanwhile, the symmetrical-equivalent A2 site, which is less perturbed, becomes a new host for majority-spin electrons, showing enhanced spin polarization. Concurrently, minority-spin states at both A1 and A2 are destabilized, as seen by the reduced ELF signal. These expelled electrons preferentially relocate to the nearby IAEs-B (B1) site, where the local potential is more favorable and exchange energy costs are low. As a result, spin density becomes highly asymmetric, with A2 dominating in majority-spin population and exhibiting amplified local magnetization.

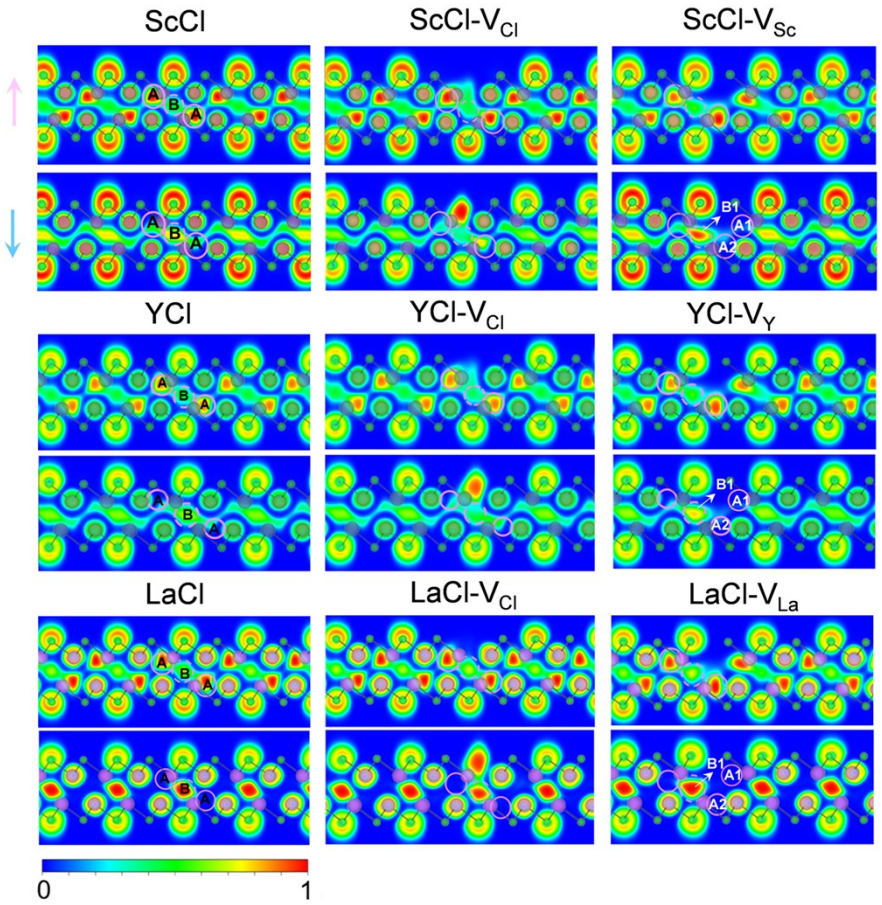

Fig. S2 IAEs distributions on pristine and defective XCl. Electron localization function (ELF) maps on the (110) plane for majority-spin (upper panel) and minority-spin (lower panel) electrons in XCl (left), XCl-V_{Cl} (middle) and XCl-V_X (right), a cropped regional view of the 5×5 computational supercell. Interstitial anionic electrons (IAEs) occupy

two distinct sites, labeled A and B, highlighted by solid and dashed pink circles, respectively.

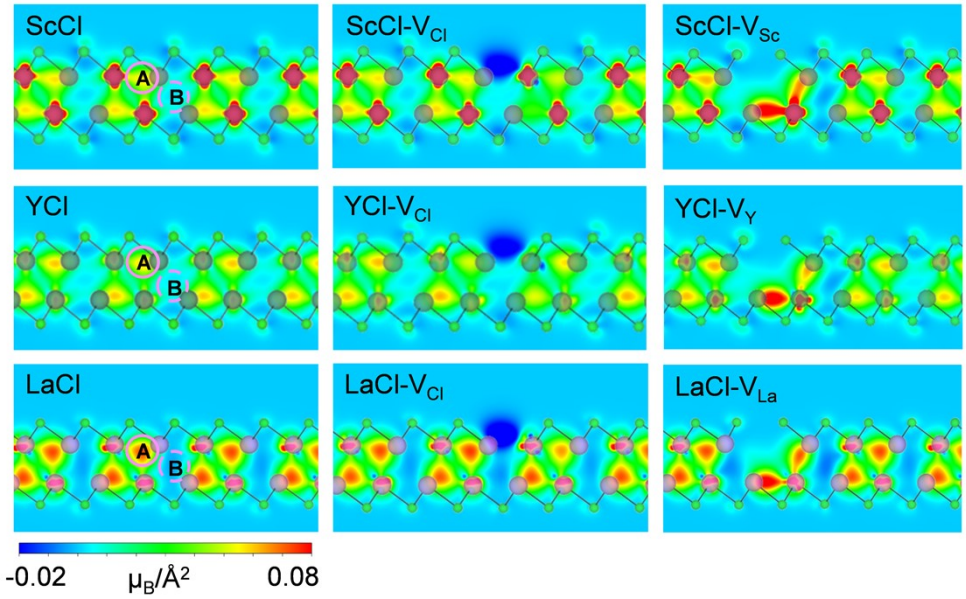

Fig. S3 Spin density plots on the (110) plane for pristine and defective XCl, a cropped regional view of the 5×5 computational supercell. From left to right: XCl, XCl-V_{Cl} and XCl-V_X. IAE-A and IAE-B are highlighted by solid and dashed pink circles, respectively.

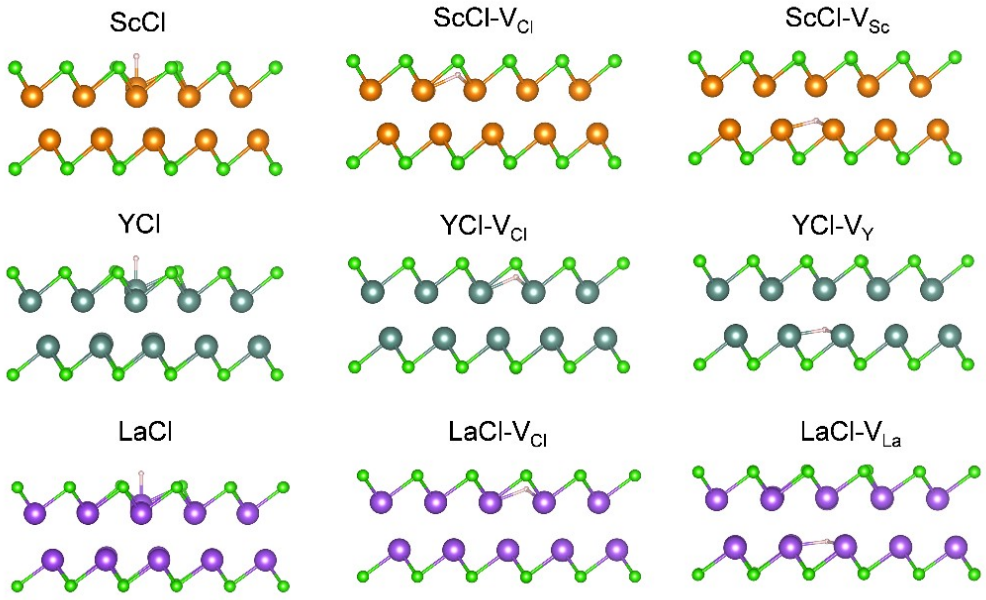

Fig. S4 H adsorption configurations of pristine and defective XCl. The orange, olive-

green, purple, green and pink circles represent Sc, Y, La, Cl, and H atoms, respectively.

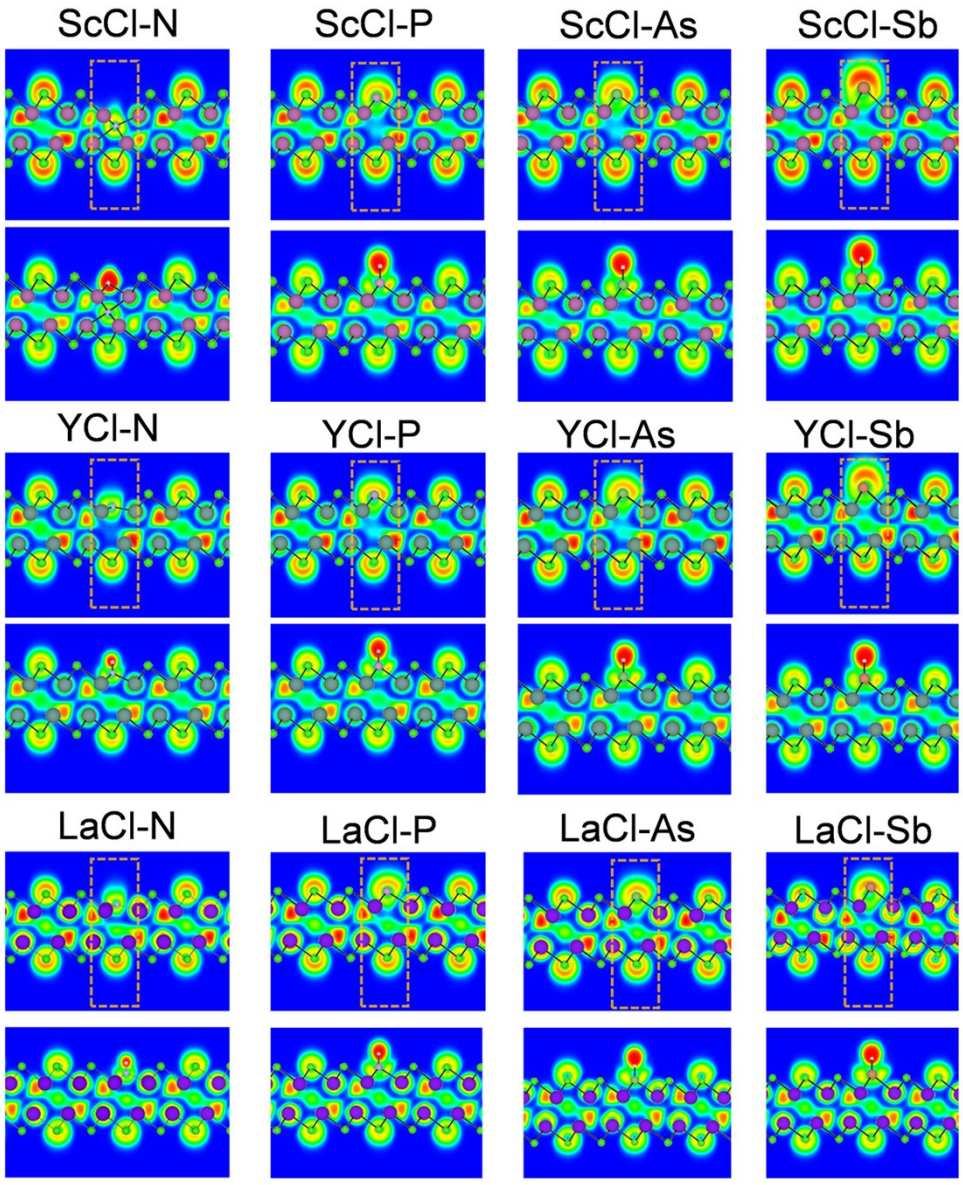

Fig. S5 IAEs distributions on single-atom doped XCl (XCl-SA) before and after H adsorption. ELF maps on the (110) plane for XCl-SA (upper panel) and XCl-SA with H adsorption (lower panel). The perturbed IAE regions are highlighted by orange dashed lines.

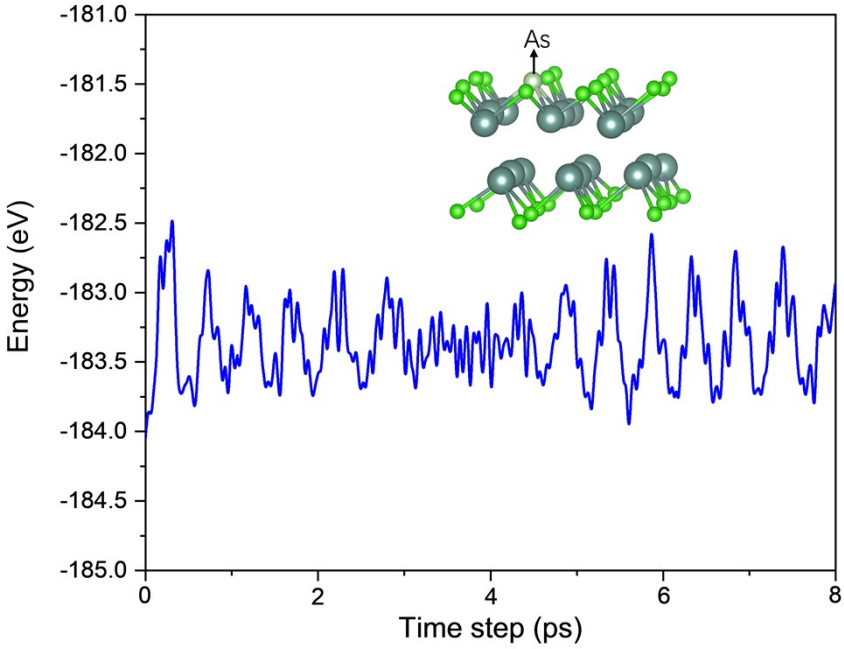

Fig. S6 Ab initio molecular dynamics (AIMD) simulations of 3×3 YCl–As at 300 K, showing the thermal stability of the doped YCl over an 8 ps trajectory.

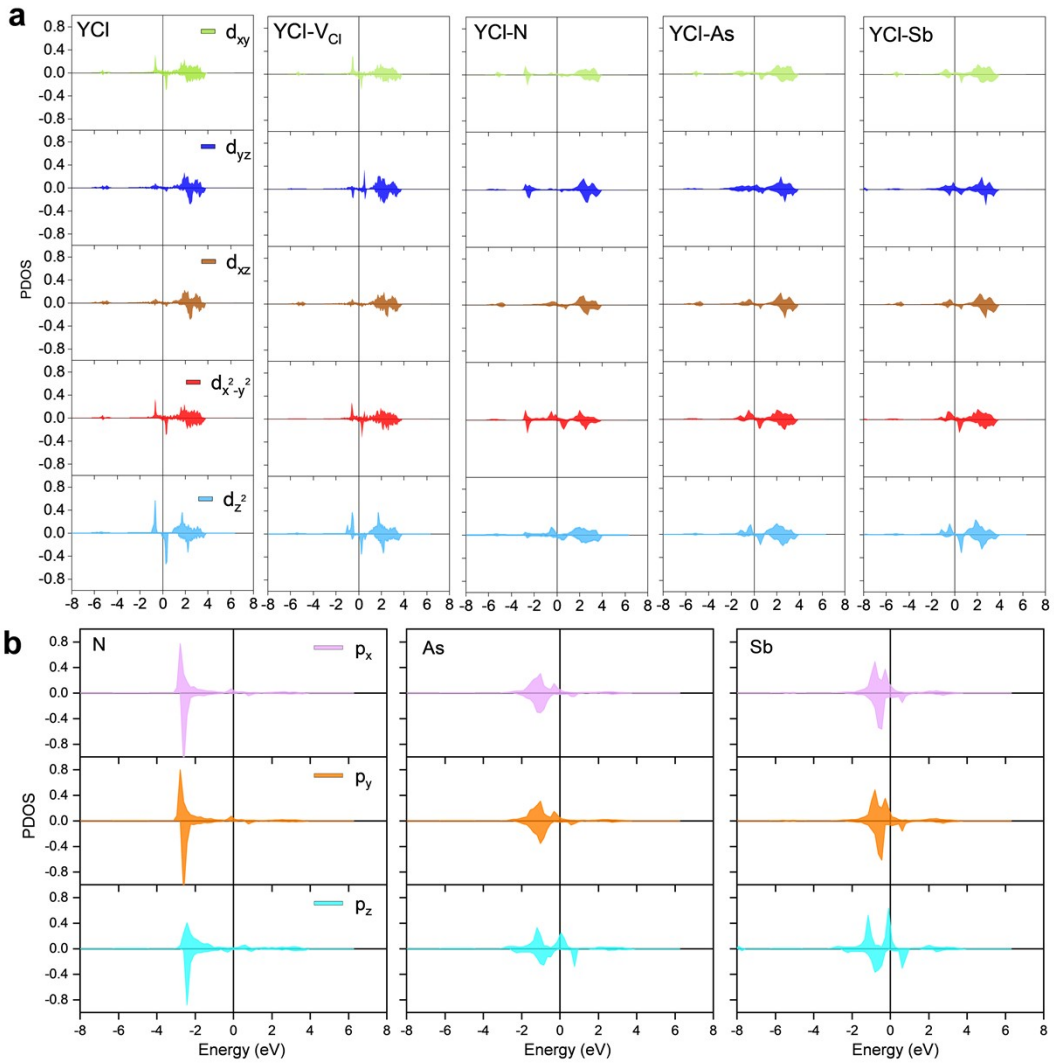

Fig. S7 PDOS of pristine and defective YCl. (a) *d* orbitals for Y. (b) *p* orbitals for N, As and Sb dopants.

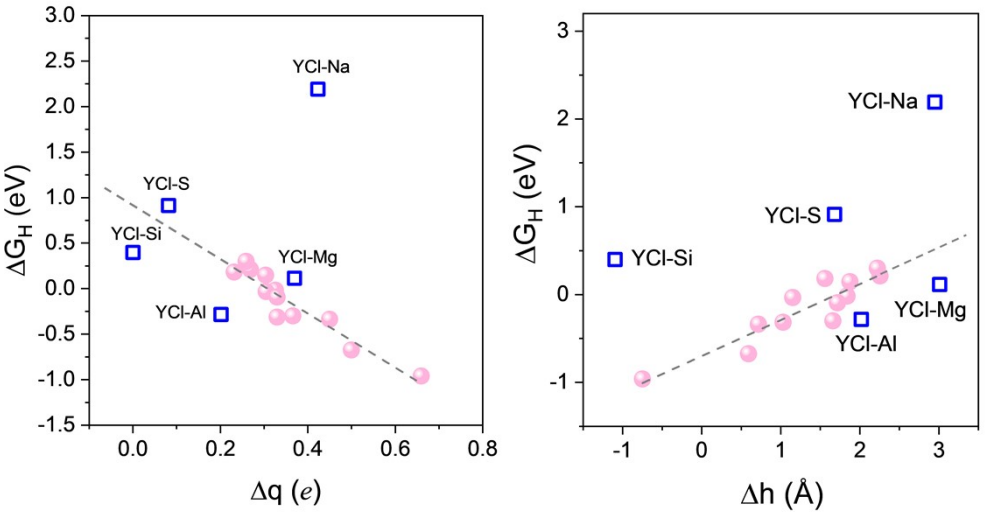

Fig. S8 Correlations of Δq and Δh with ΔG_H for Group-15 dopants in XCl systems (pink circles). Additional dopants (Na, Mg, Al, Si, S) in YCl are shown as blue squares for comparison.

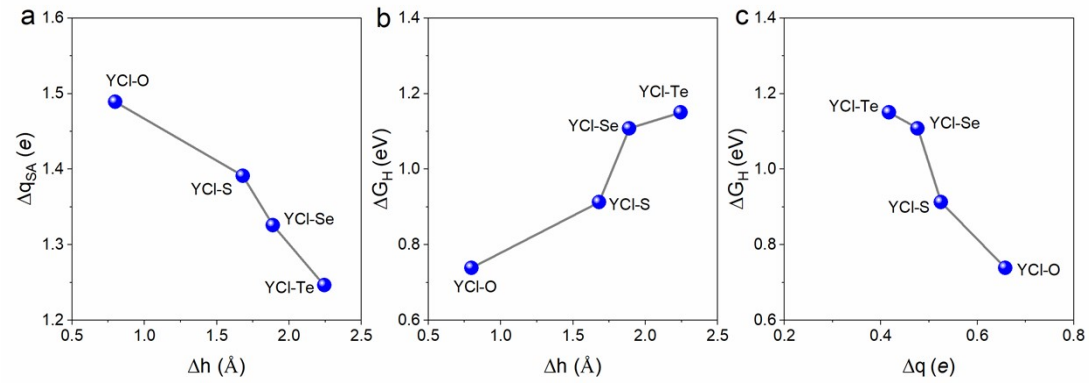

Fig. S9 Correlations of (a) Δh and Δq_{SA}, (b) Δh and ΔG_H, (c) Δq and ΔG_H for Group-16 dopants in YCl systems.

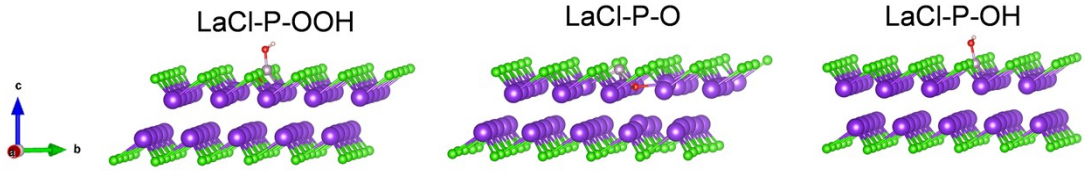

Fig. S10 ORR intermediates (*OOH, *O, and *OH) adsorption configurations. Top, middle, and bottom panels for ScCl-As, YCl-As and LaCl-P, respectively.

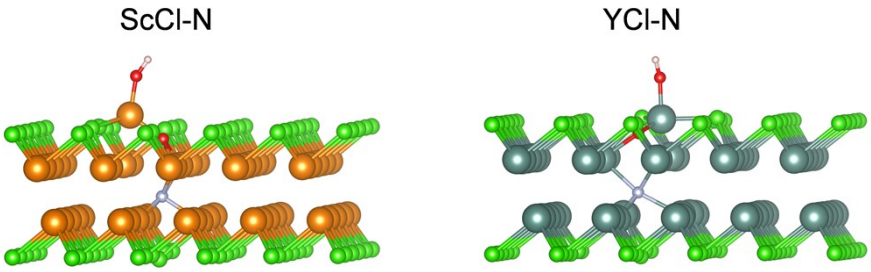

Fig. S11 Optimized adsorption configurations of *OOH on N-doped ScCl and YCl.

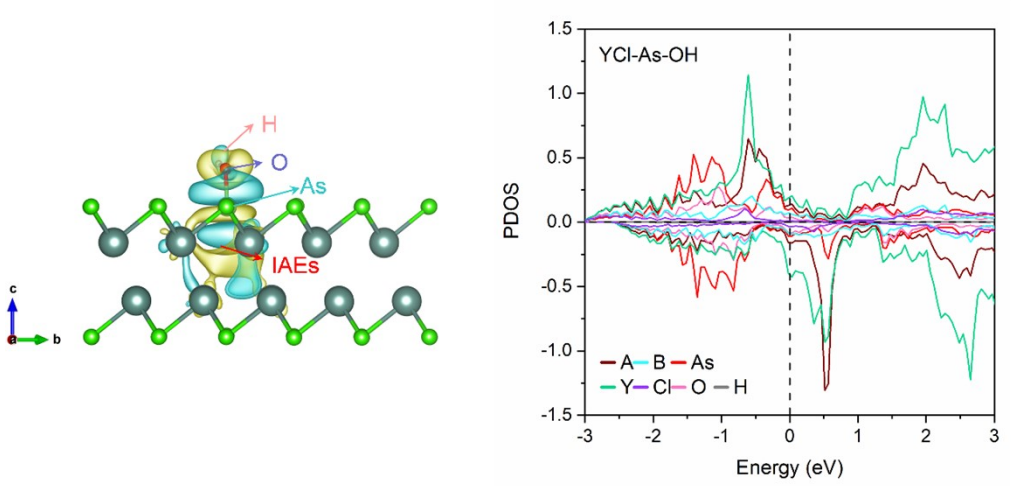

Fig. S12 Electronic properties of YCl-As with OH adsorption. Differential charge density (isosurface = 0.001 *e*/bohr^3) map on the (110) plane (left panel) and PDOS plot (right panel).

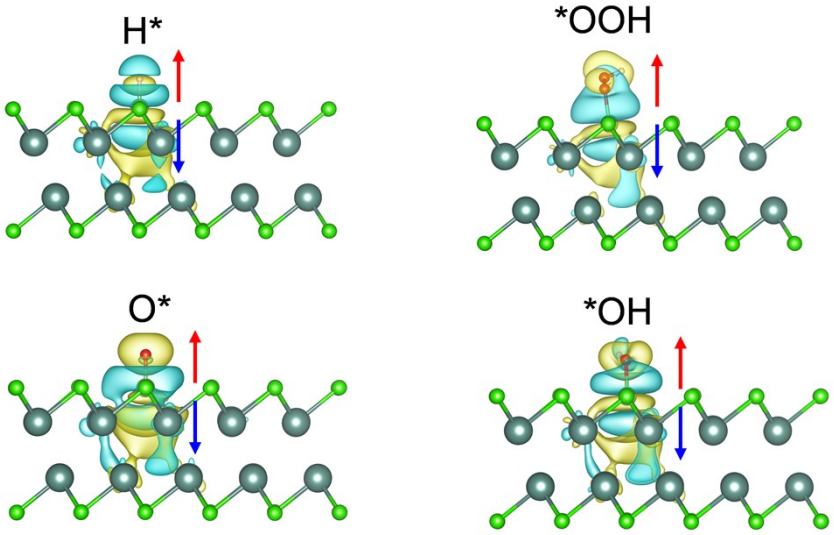

Fig. S13 Differential charge density of adsorbed intermediates (H*, *OOH, *O, and *OH) and YCl-As substrate. Arrows indicate the directions of charge transfer.

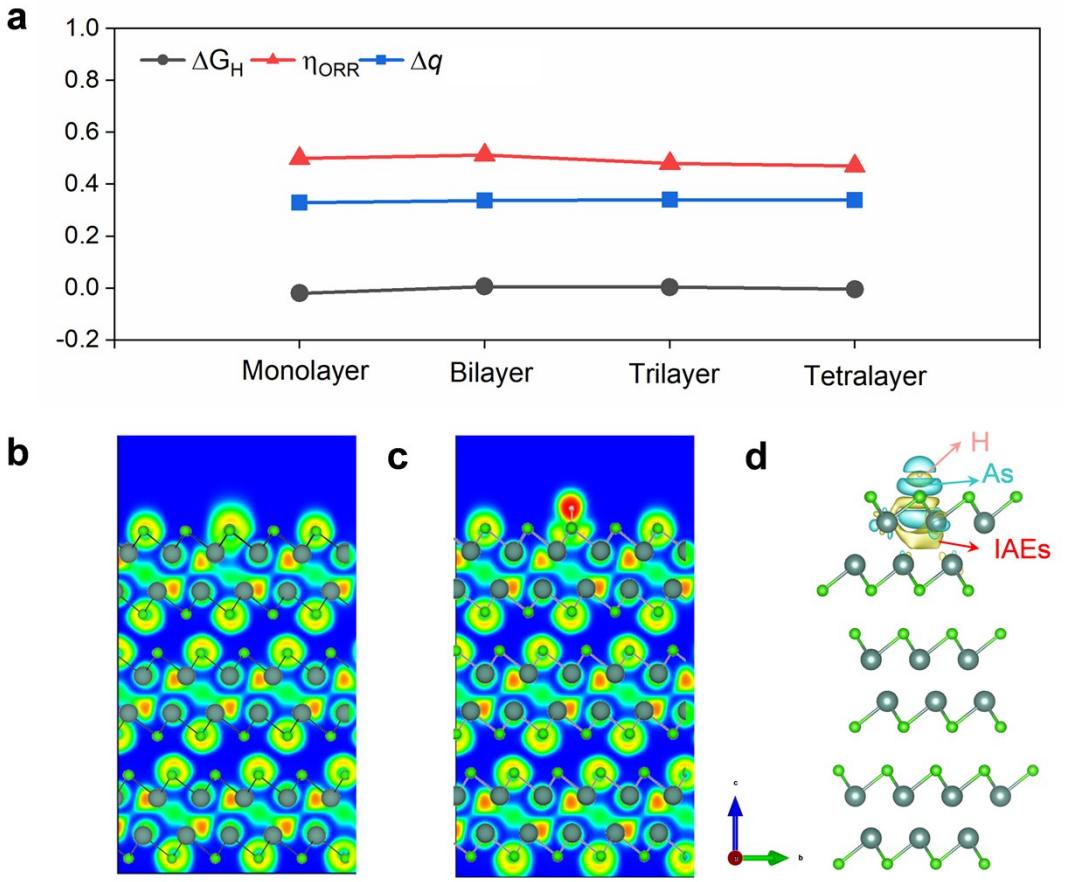

Fig. S14 Catalytic properties of multilayer YCl-As. (a) The ΔG_H, η_{ORR} and Δq values for YCl-As with different layers. (b), (c) ELF map of (110) panel in trilayer YCl-As and trilayer YCl-As with H adsorption. d, Differential charge density map of trilayer YCl-As with H adsorption. The isosurface is 0.001 *e*/bohr^3.

Table S1 Structural, energetic, magnetic and adsorption properties of pristine and defective XCl. Spin-polarized ICOHP value in XCl, XCl-V_{Cl}, XCl-V_X, bulk materials with typical chemical bonding natures, and representative 2D materials; Vacancy formation energy ($\Delta E_{F\text{-}V}$) and vacancy migration energy barrier ($\Delta E_{B\text{-}V}$) for XCl, XCl-V_{Cl}, XCl-V_X, and representative 2D materials; Magnetic moment per X atom (M); H adsorption energy (ΔE_H) for XCl, XCl-V_{Cl} and XCl-V_X. The $\Delta E_{F\text{-}V}$ and $\Delta E_{B\text{-}V}$ numbers in square brackets are taken from literatures.

	ICOHP Spin-up (down)	$\Delta E_{F\text{-}V}$ (eV)	$\Delta E_{B\text{-}V}$ (eV)	M (μ_B)	ΔE_H (eV)
ScCl	-0.74 (-0.78)	\	\	0.69	1.97
ScCl-V_{Cl}	-0.72(-0.75)	3.67	0.61	0.67	-1.16
ScCl-V_{Sc}	-0.96 (-1.09)	2.28	0.72	0.70	-1.29
YCl	-0.9 (-0.95)	\	\	0.69	1.43
YCl-V_{Cl}	-0.9 (-0.94)	3.71	0.32	0.65	-1.09
YCl-V_Y	-1.19 (-1.34)	2.16	0.83	0.70	-1.34
LaCl	-0.67 (-0.77)	\	\	0.92	0.96
LaCl-V_{Cl}	-0.67 (-0.79)	3.96	0.43	0.90	-1.09
LaCl-V_Y	-0.90 (-1.07)	2.07	0.76	0.92	-1.31
NaCl	-0.30 (-0.30)	\	\	\	\
Diamond	-4.84 (-4.84)	\	\	\	\
Fe	-0.59 (-0.91)	\	\	\	\
Graphene	-4.77 (-4.8)	\	\	\	\
Graphene-V_C	\	7.5 [7.5]	[1.3]	\	\
h-BN	-4.25 (-4.25)	\	\	\	\
h-BN-V_B(V_N)	\	[10.88 (8.81)]	[3.3 (6.1)]	\	\
MoS_2	-1.56 (-1.56)	\	\	\	\
MoS_2-V_S	\	2.48 [2.35]	2.33 [2.32]	\	\

Table S2 Structural, energetic, magnetic, electronic and adsorption properties of SA doped XCl. SA-X bond length (d_{SA-X}); SA dopant formation energy (ΔE_{F-SA}); The charge transfer of single atom dopant in XCl (Δq_{SA}); Magnetic moment of SA-doped XCl relative to XCl with V_{Cl} (ΔM); The charge transfer of single atom dopant in XCl after H adsorption (Δq_{SA-H}); The charge transfer of the adsorbed H (Δq_H); Net charge transfer between the H-SA unit and the surrounding lattice ($\Delta q = |\Delta q_{SA-H} + \Delta q_H|$) and H adsorption energies (ΔE_H) in XCl-SA.

	d_{SA-X} (Å)	ΔE_{F-SA} (eV)	Δq_{SA} (*e*)	ΔM (μ_B)	Δq_{SA-H} (*e*)	Δq_H (*e*)	Δq (*e*)	ΔE_H (eV)
ScCl-N	2.21	-5.07	+2.20	-1.42	-0.03	+0.69	0.66	-1.12
ScCl-P	2.49	-0.88	+1.52	0.87	-0.72	+0.39	0.33	-0.48
ScCl-As	2.59	-0.66	+1.43	0.89	-0.48	+0.17	0.31	-0.17
ScCl-Sb	2.85	0.07	+1.22	2.19	-0.46	+0.23	0.23	0.10
YCl-N	2.19	-3.90	+1.90	0.08	-0.16	-0.34	0.50	-0.93
YCl-P	2.68	-1.01	+1.67	1.10	-0.71	+0.34	0.37	-0.45
YCl-As	2.78	-0.89	+1.58	1.22	-0.51	+0.18	0.33	-0.14
YCl-Sb	3.03	-0.36	+1.42	2.15	-0.49	+0.22	0.27	0.13
LaCl-N	2.28	-4.52	+1.75	-0.33	-0.13	-0.32	0.45	-0.58
LaCl-P	2.78	-1.61	+1.53	0.14	-0.72	+0.40	0.33	-0.23
LaCl-As	2.89	-1.50	+1.45	0.23	-0.49	+0.19	0.30	0.04
LaCl-Sb	3.13	-0.97	+1.31	0.33	-0.50	+0.24	0.26	0.22

Table S3 Total magnetic moment per Y atom of pristine and defected YCl systems with different supercell sizes.

Total magnetic moment (M)/per Y atom	3x3 supercell	4x4 supercell	5x5 supercell
Pristine	0.62	0.69	0.69
V_{Cl}	0.57	0.65	0.67
V_Y	0.71	0.64	0.68
YCl-As	0.70	0.61	0.69

Table S4 Dopant formation energy ($\Delta E_{F\text{-}SA}$), charge transfer of the As dopant (Δq_{SA}), adsorption energies of H and OH (ΔE_H and ΔE_{OH}), and the corresponding charge transfer between the H/OH–SA unit and the surrounding lattice (Δq) in As-doped YCl systems with different supercell sizes.

YCl-As	3x3 supercell	4x4 supercell	5x5 supercell
$\Delta E_{F\text{-}SA}$	-0.85	-0.81	-0.89
Δq_{SA}	1.56	1.57	1.58
ΔE_H (Δq)	-0.14 (0.34)	-0.13 (0.34)	-0.14 (0.33)
ΔE_{OH} (Δq)	0.55 (0.33)	0.57 (0.33)	0.58 (0.34)

Table S5 Adsorption free energies (ΔG_{OOH}, ΔG_O, and ΔG_{OH}) for Group-15 single-atom-doped ScCl and YCl systems.

	ΔG_{OOH}	ΔG_O	ΔG_{OH}
ScCl-N	/	-2.85	-2.67
ScCl-P	3.46	0.64	0.20
ScCl-As	3.90	1.69	0.62
ScCl-Sb	4.00	1.90	0.63
YCl-N	/	-3.62	-3.41
YCl-P	3.53	0.72	0.30
YCl-As	4.03	1.79	0.73
YCl-Sb	4.03	2.04	0.72